J|A|C|S
ARTICLES

Published on Web 04/23/2009

Fluorescent J-Aggregates of Core-Substituted Perylene Bisimides: Studies on Structure−Property Relationship, Nucleation−Elongation Mechanism, and Sergeants-and-Soldiers Principle

Theo E. Kaiser, Vladimir Stepanenko, and Frank Würthner*

Universität Würzburg, Institut für Organische Chemie and Röntgen Research Center for Complex Material Systems, Am Hubland, 97074 Würzburg, Germany

Received January 28, 2009; E-mail: wuerthner@chemie.uni-wuerzburg.de

Abstract: A series of highly soluble and fluorescent, at core tetraaryloxy-substituted and in imide positions hydrogen atom containing perylene bisimide (PBI) dyes **1a**−**e** with varying peripheral side chains have been synthesized and thoroughly characterized. The self-assembly of these PBIs has been studied in detail by UV/vis, linear dichroism (LD) and circular dichroism (CD) spectroscopy, and scanning probe microscopy (AFM, STM). These studies revealed that the present PBIs self-assemble into extended double string cables, which consist of two hydrogen-bonded supramolecular polymeric chains of densely packed and strongly excitonically coupled PBI chromophores, providing highly fluorescent J-aggregates. The aggregation strength ("melting" temperature) and the fluorescence properties of these J-aggregates are dependent on the number and chain length of the peripheral alkoxy substituents, thus revealing a structure−property relationship. In contrast to previously reported assemblies of PBIs, for which the aggregation process is described by the isodesmic (or equal *K*) model, a cooperative nucleation−elongation mechanism applies for the aggregation of the present assemblies as revealed by concentration-dependent UV/vis absorption studies with the chiral PBI **1e**, providing equilibrium constants for dimerization (= nucleation) of $K_2 = 13 \pm 11$ L mol^{-1} and for elongation of $K = 2.3 \pm 0.1 \times 10^6$ L mol^{-1} in methylcyclohexane (MCH). LD spectroscopic measurements have been performed to analyze the orientation of the monomers within the aggregates. The nonlinearity of chiral amplification in PBI aggregates directed by sergeants-and-soldiers principle has been elucidated by coaggregation experiments of different PBI dyes using CD spectroscopy. The dimensions as well as the molecular arrangement of the monomeric units in assemblies have been explored by atomic force microscopy (AFM) and scanning tunneling microscopy (STM).

Introduction

J-aggregates (also called Scheibe aggregates) were discovered independently by Jelley and Scheibe during their studies with cyanine dyes more than 70 years ago.[1] It was observed that at higher concentrations of pseudo-isocyanine dye a new, very narrow absorption band appears which is red-shifted with respect to that of the monomer dye, and a narrow resonance fluorescence band with small Stokes shift was observed as well. Scheibe ascribed this phenomenon to a reversible polymerization of the chromophores.[1c−f] Presently, it is generally agreed that the molecules in these dye aggregates are bound to each other by noncovalent van-der-Waals interactions and are highly ordered in a slipped arrangement.[2−4] Due to a strong coupling between transition dipole moments of the constituent molecules, excitonic states are created by optical excitation that results in such characteristic spectral features, i.e., narrow and bathochromically shifted absorption band and high fluorescence quantum yield.[2b]

(1) (a) Jelley, E. E. *Nature (London)* **1936**, *138*, 1009–1010. (b) Jelley, E. E. *Nature (London)* **1937**, *139*, 631–632. (c) Scheibe, G. *Angew. Chem.* **1936**, *49*, 563. (d) Scheibe, G. *Angew. Chem.* **1937**, *50*, 51. (e) Scheibe, G. *Kolloid-Z.* **1938**, *82*, 1–14. (f) Scheibe, G.; Schöntag, A.; Katheder, F. *Naturwissenschaften* **1939**, *29*, 499–501.

(2) For reviews on cyanine J-aggregates, see: (a) Möbius, D. *Adv. Mater.* **1995**, *7*, 437–444. (b) Kobayashi, T., Ed. *J-Aggregates*; World Science: Singapore, 1996. (c) Dähne, S. *Bunsen-Magazin* **2002**, *4*, 81–92. (d) Knoester, J. *Int. J. Photoenergy* **2006**, *5*, 4(1−10). (e) Kirstein, S.; Daehne, S. *Int. J. Photoenergy* **2006**, *5*, 3(1−21). (f) Shapiro, B. I. *Russ. Chem. Rev.* **2006**, *75*, 433–456. (g) Egorov, V. V.; Alfimov, M. V. *Phys.-Usp.* **2007**, *50*, 985–1029.

(3) For a selection of theoretical work on cyanine J-aggregates, see: (a) Fidder, H.; Knoester, J.; Wiersma, D. A. *J. Chem. Phys.* **1991**, *95*, 7880–7890. (b) Tuszyński, J. A.; Jørgensen, M. F.; Möbius, D. *Phys. Rev. E* **1999**, *59*, 4374–4383. (c) Bednarz, M.; Malyshev, V. A.; Knoester, J. *Phys. Rev. Lett.* **2003**, *91*, 217401(1−4). (d) Walczak, P. B.; Eisfeld, A.; Briggs, J. S. *J. Chem. Phys.* **2008**, *128*, 044505(1−12). and refs 2d and g.

(4) Recent publications on cyanine J-aggregates: (a) Czikkely, V.; Försterling, H. D.; Kuhn, H. *Chem. Phys. Lett.* **1970**, *6*, 11–14, and 207−210. (b) Scheibe, G.; Haimerl, F.; Hoppe, W. *Tetrahedron Lett.* **1970**, *11*, 3067–3070. (c) Daltrozzo, E.; Scheibe, G.; Geschwind, K.; Haimerl, F. *Photogr. Sci. Eng.* **1974**, *18*, 441–450. (d) Herz, A. H. *Photogr. Sci. Eng.* **1974**, *18*, 323–335. (e) Herz, A. H. *Adv. Colloid Interface Sci.* **1977**, *8*, 237–298. (f) Sundström, V.; Gilbro, T.; Gadonas, R. A.; Piskarskas, A. *J. Chem. Phys.* **1988**, *89*, 2754–2762. (g) Higgins, D. A.; Barbara, P. F. *J. Phys. Chem.* **1995**, *99*, 3–7. (h) von Berlepsch, H.; Böttcher, C.; Dähne, L. *J. Phys. Chem. B* **2000**, *104*, 8792–8799. (i) Scheblykin, I. G.; Sliusarenko, O. Y.; Lepnev, L. S.; Vitukhnovsky, A. G.; Van der Auweraer, M. *J. Phys. Chem. B* **2001**, *105*, 4636–4646. (j) Rousseau, E.; Koetse, M. M.; Van der Auweraer, M. *Photochem. Photobiol. Sci.* **2002**, *1*, 395–406. (k) Pawlik, A.; Ouart, A.; Kirstein, S.; Abraham, H.-W.; Daehne, S. *Eur. J. Org. Chem.* **2003**, 3065–3080, and ref 2e.

Scheme 1. Self-Assembly of PBI Dyes by Double Hydrogen-Bonding Motif

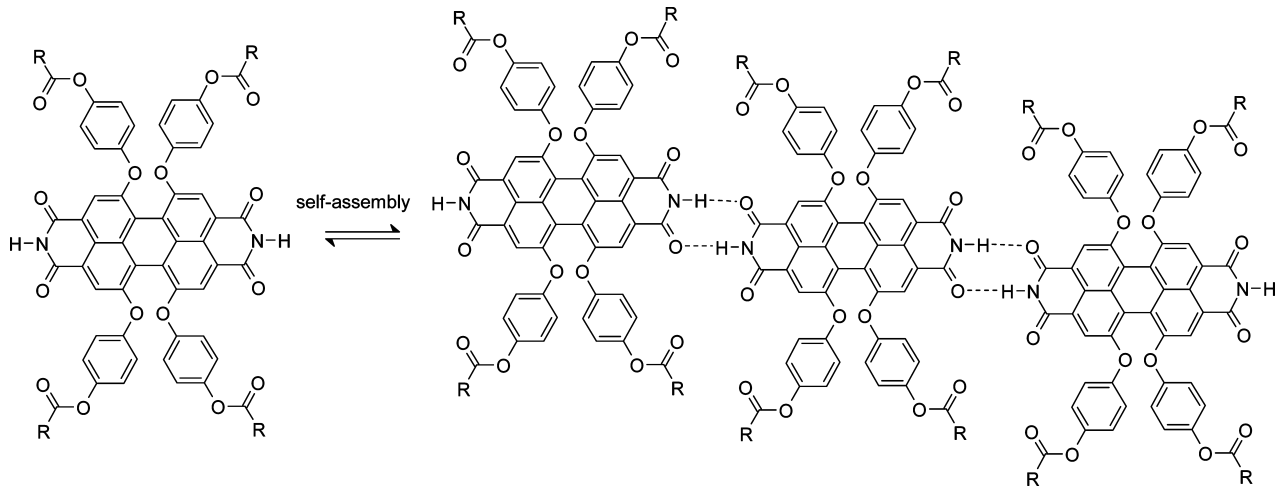

Chart 1. Structures of PBI Dyes **1a**−**e** Investigated Here

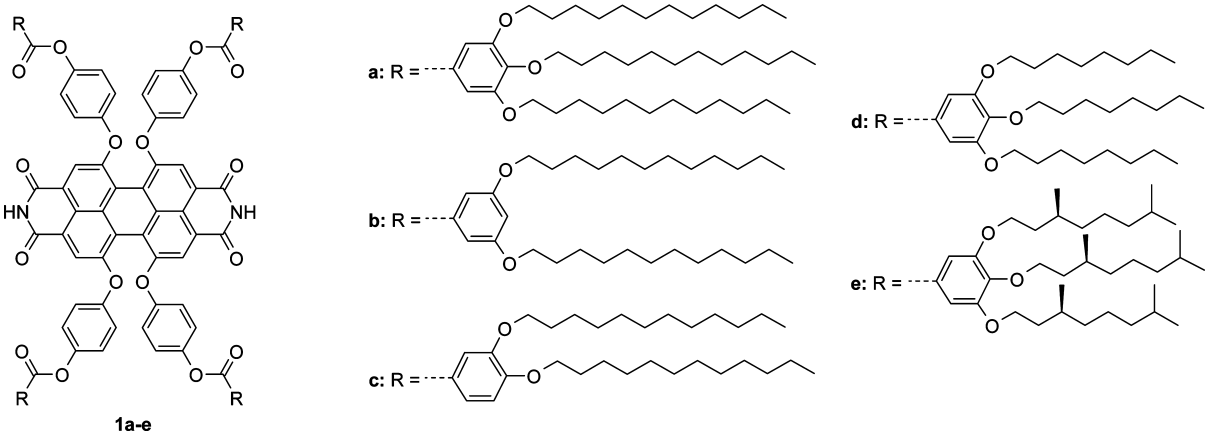

J-aggregates of cyanine dyes have attracted scientific interest, and they play an important role in many technological applications.[2a,d,5] For example, due to their strong absorption such J-aggregates have been applied for the sensitization of the photographic process with silver halides.[4e,6] In recent years, they have received considerable attention as fluorescent sensors,[7] organic photoconductors,[8] and organic photovoltaic materials[9] due to their exciton transport capabilities.

Dye aggregates with a slipped arrangement and concomitant exciton delocalization properties are promising for artificial light harvesting.[10] In natural light-harvesting systems, a slipped arrangement of chlorophyll dyes is accomplished by proteins or metal-ion coordination, providing J-type aggregates.[11] To mimic natural archetype, structurally related porphyrin dyes have been designed that self-assemble in J-type packing.[12] However, since these chromophores exhibit much less favorable optical properties, especially a rather weak photoluminescence resulting from an almost forbidden lowest-energy transition, porphyrin aggregates can compete in this regard neither with their natural chlorophyll counterparts nor with cyanine dye-based synthetic J-aggregates. Despite enormous efforts that had been invested during the last decades, further examples of other dye aggregates with optical properties similar to those of cyanine dye aggregates could be barely achieved.[10a,13] Many synthetic π-conjugated dyes, including perylene bisimides (PBIs), form preferentially sandwich-type H-aggregates that exhibit unfavorable, strongly quenched fluorescence properties.[14,15] This infers, particularly in the case of PBIs, from the strong dispersion and quadrupolar interactions of the mostly flat perylene core that affords rotational instead of longitudinal displacements in columnar π-stacks.[15a,d] Perylene bisimide dyes are remarkably photostable and monomeric PBIs are highly fluorescent, they exhibit fairly

(5) (a) Kuhn, H.; Kuhn, C. In *J-Aggregates*; Kobayashi, T., Ed.; World Scientific: Singapore, 1996; pp 1−40. (b) Pawlik, A.; Kirstein, S.; De Rossi, U.; Dähne, S. *J. Phys. Chem. B* **1997**, *101*, 5646–5651.
(6) (a) Herz, A. H. *The Theory of the Photographic Process*, 4th ed.; James, T. H., Ed.; MacMillan: New York, 1977; Chapter 9 and references therein.
(7) (a) Hannah, K. C.; Armitage, B. A. *Acc. Chem. Res.* **2004**, *37*, 845–853. (b) Whitten, D. G.; Achyuthan, K. E.; Lopez, G. P.; Kim, O.-K. *Pure Appl. Chem.* **2006**, *78*, 2313–2323.
(8) Law, K. Y. *Chem. Rev.* **1993**, *93*, 449–86.
(9) (a) Meng, F.; Chen, K.; Tian, H.; Zuppiroli, L.; Nuesch, F. *Appl. Phys. Lett.* **2003**, *82*, 3788–3790. (b) Sayama, K.; Tsukagoshi, S.; Mori, T.; Hara, K.; Ohga, Y.; Shinpou, A.; Abe, Y.; Suga, S.; Arakawa, H. *Sol. Energy Mater. Sol. Cells* **2003**, *80*, 47–71. (c) Kawasaki, M.; Aoyama, S. *Chem. Commun.* **2004**, 988–989. (d) Tameev, A. R.; Vannikov, A. V.; Schoo, H. F. M. *Thin Solid Films* **2004**, *451/452*, 109–111.
(10) (a) Hoeben, F. J. M.; Jonkheim, P.; Meijer, E. W.; Schenning, A. P. H. J. *Chem. Rev.* **2005**, *105*, 1491–1546. (b) Wasielewski, M. R. *J. Org. Chem.* **2006**, *71*, 5051–5066. (c) Yamamoto, Y.; Fukushima, T.; Suna, Y.; Ishii, N.; Saeki, A.; Seki, S.; Tagawa, S.; Taniguchi, M.; Kawai, T.; Aida, T. *Science* **2006**, *314*, 1761–1764. (d) Miller, R. A.; Presley, A. D.; Francis, M. B. *J. Am. Chem. Soc.* **2007**, *129*, 3104–3109.
(11) (a) *Photosynthetic Light-Harvesting Systems: Organization and Function*; Scheer, H.; Schneider, S., Eds.; de Gruyter: Berlin, 1988. (b) Prokhorenko, V. I.; Steensgard, D. B.; Holzwarth, A. R. *Biophys. J.* **2000**, *79*, 2105–2120.

persistent radical anion states toward environmental influences, and are easily accessible.[16] These outstanding properties led to wide applications of perylene dyes in various fields, e.g., in bioimaging,[17] single molecule spectroscopy (SMS),[16a,18] organic solar cells[19] and field-effect transistors (OFETs),[20] and in organic and polymeric light-emitting diodes (OLEDs and PLEDs).[21]

The aim of the present work was to obtain PBI aggregates that do not assemble in commonly observed H-type, but rather in J-type fashion yielding highly fluorescent supramolecular systems. We thought that intermolecular hydrogen bonding of monomeric PBI units, in addition to the $\pi-\pi$-stacking interactions, may enable a slipped arrangement to obtain J-aggregates (see Scheme 1). Introduction of bulky substituents at the so-called bay area of the perylene core (1,6,7,12 positions) should prevent sandwich-type stacking and enforce the monomers to a longitudinal displacement with respect to another. Indeed, this concept provided the first perylene bisimide J-aggregate with a narrow J-band and a fluorescence quantum yield of nearly unity as we have recently communicated.[22a] In this communication, we have reported that PBI **1a** (for structure, see Chart 1), designed by above-mentioned concept, self-assembles in aliphatic solvents like methylcyclohexane (MCH) into one-dimensional aggregates with characteristic spectral features of J-type arrangement that was analyzed by temperature-dependent absorption and fluorescence spectroscopy, and atomic force microscopy (AFM). The existence of hydrogen bonds could be evidenced by temperature- and concentration-dependent ^{1}H NMR as well as FT-IR spectroscopy in different solvents.[22a] In the meanwhile, other J-aggregates based on PBI dyes have been reported in the literature which were achieved by hydrogen bonding assisted by amide groups,[23a] addition of cyanuric acid derivative,[23b] and by changing the solvent polarity.[23c] However, in contrast to cyanine and chlorin J-aggregates, these PBI aggregates exhibit rather broad J-bands which coexist with an additional absorption band that in most cases is hypsochromically shifted.[23]

Herein we report our detailed studies on self-assembly of a series of core-tetrasubstituted perylene bisimides **1a**−**e**, including a chiral derivative **1e**, into J-aggregates (Scheme 1 and Chart 1). Theoretical calculations were performed based on Kasha's exciton model[24] to rationalize the observed spectral shifts in absorption. By using the chiral PBI **1e**, we have elucidated for the first time the nucleation−elongation mechanism in self-assembly of PBIs. Nucleation elongation is a cooperative supramolecular polymerization mechanism that is ubiquitous in biology, typically for the formation of helical or tubular structures, and has been studied, e.g., for actin, tubulin, bacterial flagellin, and tobacco mosaic virus.[25,26] This mechanism assumes a cooperative growth of the chain that is initiated by a less favored formation of a nucleus, followed by an highly

(12) (a) Takahashi, R.; Kobuke, Y. *J. Am. Chem. Soc.* **2003**, *125*, 2372–2373. (b) Yamaguchi, T.; Kimura, T.; Matsuda, H.; Aida, T. *Angew. Chem., Int. Ed.* **2004**, *43*, 6350–6355. (c) Elemans, J. A. A. W.; van Hameren, R.; Nolte, R. J. M.; Rowan, A. E. *Adv. Mater.* **2006**, *18*, 1251–1266.

(13) (a) Ajayaghosh, A.; George, S. J.; Schenning, A. P. H. J. *Top. Curr. Chem.* **2005**, *258*, 83–118. For a review on phosphorescent assemblies, see: (b) Bruzzone, L.; Badia, R.; Diaz Garcia, M. E. *Crit. Rev. Anal. Chem.* **2000**, *30*, 163–178.

(14) Würthner, F. *Chem. Commun.* **2004**, 1564–1579.

(15) Some fluorescent aggregates of perylene bisimides have been reported, but they do not display J-type characteristics such as small Stokes shift and narrow emission bands: (a) Würthner, F.; Thalacker, C.; Diele, S.; Tschierske, C. *Chem.−Eur. J.* **2001**, *7*, 2245–2253. (b) De Feyter, D.; Liu, S.; Cotlet, M.; Wiesler, U.-M.; Weil, T.; Herrmann, A.; Müllen, K.; De Schryver, F. C. *Macromolecules* **2003**, *36*, 8489–8498. (c) Yan, P.; Chowdhury, A.; Holman, M. W.; Adams, D. M. *J. Phys. Chem. B* **2005**, *109*, 724–730. (d) Chen, Z.; Stepanenko, V.; Dehm, V.; Prins, P.; Siebbeles, L. D. A.; Seibt, J.; Marquetand, P.; Engel, V.; Würthner, F. *Chem.−Eur. J.* **2007**, *13*, 436–449.

(16) For current reviews on PBIs, see: ref 12c, ref 14 and (a) Grimsdale, A. C.; Müllen, K. *Angew. Chem., Int. Ed.* **2005**, *44*, 5592–5629. (b) De Schryver, F. C.; Vosch, T.; Cotlet, M.; Van der Auweraer, M.; Müllen, K.; Hofkens, J. *Acc. Chem. Res.* **2005**, *38*, 514–522. (c) Würthner, F. *Pure Appl. Chem.* **2006**, *78*, 2341–2349. In a recent account, one-dimensional self-assembly of core-unsubstituted PBIs has been described: (d) Zang, L.; Che, Y. K.; Moore, J. S. *Acc. Chem. Res.* **2008**, *41*, 1596–1608. For recent publications on the stability of radical anions of PBIs, see: (e) Marcon, R. O.; Brochsztain, S. *Langmuir* **2007**, *23*, 11972–11976. (f) Baram, J.; Shirman, E.; Ben-Shitrit, N.; Ustinov, A.; Weissman, H.; Pinkas, I.; Wolf, S. G.; Rybtchinski, B. *J. Am. Chem. Soc.* **2008**, *130*, 14966–14967.

(17) (a) Kohl, C.; Weil, T.; Qu, J.; Müllen, K. *Chem.−Eur. J.* **2004**, *10*, 5297–5310. (b) Yukruk, F.; Dogan, A. L.; Canpinar, H.; Guc, D.; Akkaya, E. U. *Org. Lett.* **2005**, *7*, 2885–2887.

(18) (a) Hofkens, J.; Vosch, T.; Maus, M.; Köhn, F.; Cotlet, M.; Weil, T.; Herrmann, A.; Müllen, K.; De Schryver, F. C. *Chem. Phys. Lett.* **2001**, *333*, 255–263. (b) Sliwa, M.; Flors, C.; Oesterling, I.; Hotta, J.; Müllen, K.; De Schryver, F. C.; Hofkens, J. *J. Phys.: Condens. Matter* **2007**, *19*, 445004(1−14). (c) Melnikov, S. M.; Yeow, E. K. L.; Uji-i, H.; Cotlet, M.; Müllen, K.; De Schryver, F. C.; Enderlein, J.; Hofkens, J. *J. Phys. Chem. B* **2007**, *111*, 708–719.

(19) (a) Kerp, H. R.; Donker, H.; Koehorst, R. B. M.; Schaafsma, T. J.; van Faassen, E. E. *Chem. Phys. Lett.* **1998**, *298*, 302–308. (b) Dittmer, J. J.; Marseglia, E. A.; Friend, R. H. *Adv. Mater.* **2000**, *12*, 1270–1274. (c) Schmidt-Mende, L.; Fechtenkötter, A.; Müllen, K.; Moons, E.; Friend, R. H.; MacKenzie, J. D. *Science* **2001**, *293*, 1119–1122. (d) Tan, L.; Curtis, M. D.; Francis, A. H. *Chem. Mater.* **2004**, *16*, 2134–2141. (e) Shin, W. S.; Jeong, H.-H.; Kim, M.-K.; Jin, S.-H.; Kim, M.-R.; Lee, J.-K.; Lee, J. W.; Gal, Y.-S. *J. Mater. Chem.* **2006**, *16*, 384–390. (f) Sommer, M.; Thelakkat, M. *Eur. Phys. J.: Appl. Phys.* **2006**, *36*, 245–249.

(20) (a) Jones, B. A.; Ahrens, M. J.; Yoon, M.-H.; Facchetti, A.; Marks, T. J.; Wasielewski, M. R. *Angew. Chem., Int. Ed.* **2004**, *43*, 6363–6366. (b) Chen, H.-Z.; Shi, M.-M.; Aernouts, T.; Wang, M.; Borghs, G.; Heremans, P. *Sol. Energy Mater. Sol. Cells* **2005**, *87*, 521–527. (c) Wang, Y.; Chen, Y.; Li, R.; Wang, S.; Su, W.; Ma, P.; Wasielewski, M. R.; Jiang, J. *Langmuir* **2007**, *23*, 5836–5842. (d) Schmidt, R.; Ling, M. M.; Oh, J. H.; Winkler, M.; Könemann, M.; Bao, Z.; Würthner, F. *Adv. Mater.* **2007**, *19*, 3692–3695.

(21) (a) Ranke, P.; Bleyl, I.; Simmer, J.; Haarer, D.; Bacher, A.; Schmidt, H. W. *Appl. Phys. Lett.* **1997**, *71*, 1332–1334. (b) Pösch, P.; Thelakkat, M.; Schmidt, H. W. *Synth. Met.* **1999**, *102*, 1110–1112. (c) Fan, L.; Zhu, W.; Li, J.; Tian, H. *Synth. Met.* **2004**, *145*, 203–210. (d) Sugiyasu, K.; Fujita, N.; Shinkai, S. *Angew. Chem., Int. Ed.* **2004**, *43*, 1229–1233. (e) Pandey, A. K.; Nunzi, J.-M. *Appl. Phys. Lett.* **2007**, *90*, 263508(1−3). (f) Jaiser, F.; Neher, D.; Meisel, A.; Nothofer, H.-G.; Miteva, T.; Herrmann, A.; Müllen, K.; Scherf, U. *J. Chem. Phys.* **2008**, *129*, 114901(1−9). For the application of PBIs in PLEDs, see: (g) Ego, C.; Marsitzky, D.; Becker, S.; Zhang, J.; Grimsdale, A. C.; Müllen, K.; MacKenzie, J. D.; Silva, C.; Friend, R. H. *J. Am. Chem. Soc.* **2003**, *125*, 437−443.

(22) (a) Kaiser, T. E.; Wang, H.; Stepanenko, V.; Würthner, F. *Angew. Chem., Int. Ed.* **2007**, *46*, 5541–5544. (b) Koenemann, M.; Wuerthner, F.; Osswald, P.; Kaiser, T. WO 2008113753 A1 20080925, PCT Int. Appl., 2008.

(23) (a) Würthner, F.; Bauer, Ch.; Stepanenko, V.; Yagai, S. *Adv. Mater.* **2008**, *20*, 1695–1698. (b) Yagai, S.; Seki, T.; Karatsu, T.; Kitamura, A.; Würthner, F. *Angew. Chem., Int. Ed.* **2008**, *47*, 3367–3371. (c) Yang, X.; Xu, X.; Ji, H.-F. *J. Phys. Chem. B* **2008**, *112*, 7196–7202. For PBI aggregates exhibiting less characteristic H-/J-bands that are attributed to rotationally displaced dyes, see refs 15a, d, and (d) Würthner, F.; Chen, Z.; Hoeben, F. J. M.; Osswald, P.; You, C.-C.; Jonkheijm, P.; von Herrikhuyzen, J.; Schenning, A. P. H. J.; van der Schoot, P. P. A. M.; Meijer, E. W.; Beckers, E. H. A.; Meskers, S. C. J.; Janssen, R. A. J. *J. Am. Chem. Soc.* **2004**, *126*, 10611–10618. (e) Jancy, B.; Asha, S. K. *Chem. Mater.* **2008**, *20*, 169–181.

(24) Kasha, M.; Rawls, H. R.; El-Bayoumi, M. A. *Pure Appl. Chem.* **1965**, *11*, 371–392.

(25) Oosawa, F.; Asakura S. *Thermodynamics of the Polymerization of Protein*; Academic Press: New York, 1975.

(26) (a) Klug, A. *Angew. Chem., Int. Ed. Engl.* **1983**, *22*, 565–582. (b) Caspar, D. L. *Biophys. J.* **1980**, *32*, 103–138. (c) van Workum, K.; Douglas, J. F. *Macromol. Symp.* **2005**, *227*, 1–16.

Scheme 2. Synthesis of PBI Dyes **1a**−**e**[a] and the Structure of Reference Compound **2a**

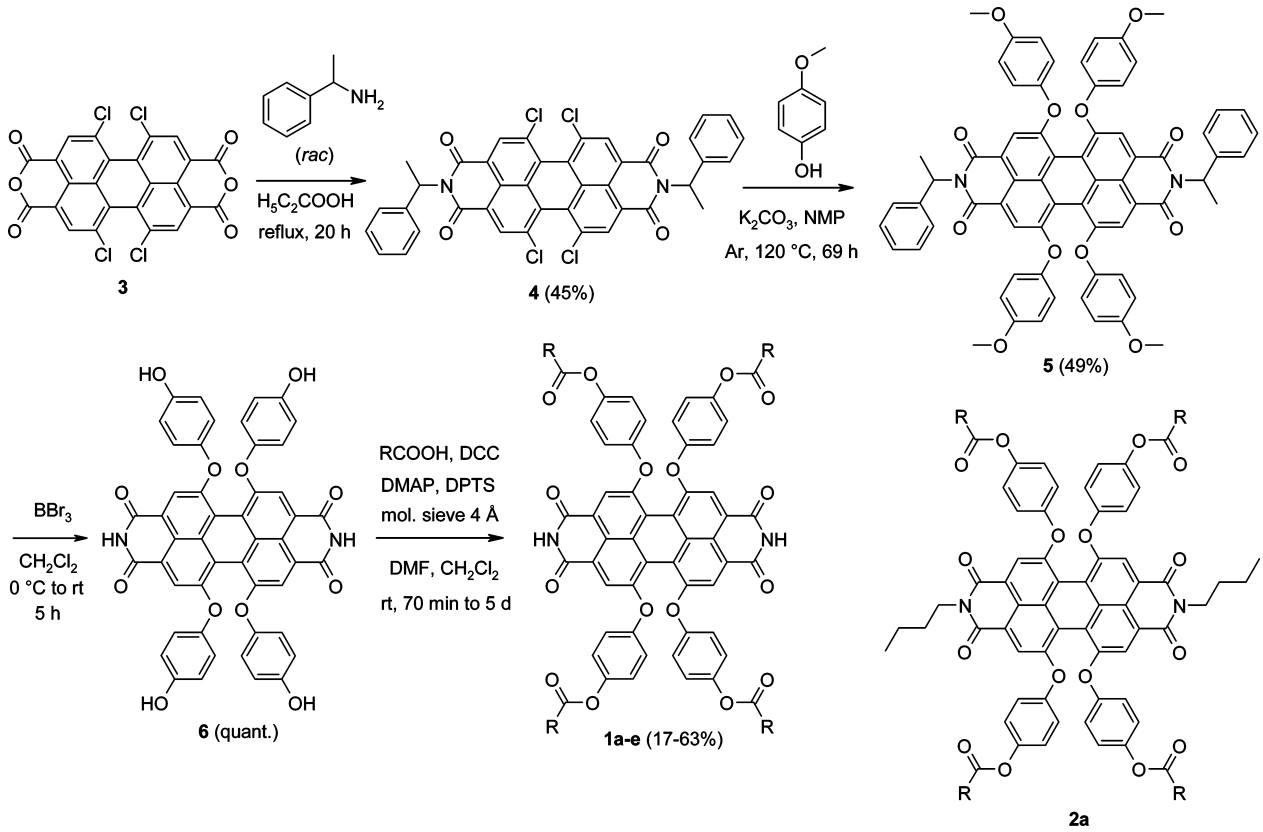

[a] NMP = *N*-methylpyrrolidone, DCC = *N,N*′-dicyclohexylcarbodiimide, DMAP = 4-dimethylaminopyridine, DPTS = 4-(dimethylamino)pyridinium 4-tosylate. For the substituents R, see Chart 1.

favored elongation of the chain.[27] We have also performed coaggregation experiments with different PBI J-aggregates and could show that the "sergeants-and-soldiers" principle[28] is applicable to PBI aggregates, which is so far unprecedented.

Results

Synthesis of PBI Dyes 1a−e. The perylene bisimide dyes **1a**−**e** (Chart 1) were synthesized from 1,6,7,12-tetrachloroperylene-3,4:9,10-tetracarboxylic acid bisanhydride (**3**) in four steps according to the route depicted in Scheme 2.[22] Imidization of **3** with racemic α-methylbenzylamine provided the soluble tetrachloro-PBI derivative **4**, which was further reacted with 4-methoxyphenol to afford perylene bisimide **5** by nucleophilic substitution of all four chlorine atoms. Treatment of **5** with BBr_3 in anhydrous CH_2Cl_2 cleaved the methyl ether groups in the bay substituents as well as the *N*-methylbenzyl groups in the imide positions in one step to give the deprotected intermediate **6**. Although PBIs with NH groups in the imide positions are of low solubility with pigment character, compound **6** is well soluble, as the four phenoxy groups in bay position provoke a twist of the perylene core. Esterification of all phenol groups in **6** with the respective alkoxybenzoic acids afforded the dyes **1a**−**e** in 17−63% yields (for further details, see the Supporting Information). The long alkyl chains in substituents R provide high solubility to the present PBIs and enable the formation of extended aggregates in nonpolar organic solvents like MCH. The reference PBI **2a** was synthesized similarly by imidization of **3** with *n*-butylamine (see Scheme S1 in the Supporting Information). The perylene bisimides **1a**−**e** and **2a** were purified by column chromatography and characterized by ^{1}H NMR and UV/vis spectroscopy, high-resolution mass spectrometry, and elemental analysis.

Spectroscopic Studies of PBI 1a−e and 2a Monomers and Their Aggregates. The UV/vis absorption as well as fluorescence spectra of monomeric dyes **1** in CH_2Cl_2 (see Figures S1−S5 in the Supporting Information) exhibit all the typical spectral features of tetraphenoxy-substituted perylene bisimide chromophores.[16c] The absorption maxima of the strongly allowed S_0-S_1 transition appear at 570−571 nm (absorption coefficients ε = 40200−41900 L mol^{-1} cm^{-1}) for PBI **1a**−**e** and the fluorescence emission spectra with maxima at λ_{max} = 598−603 nm are mirror images relative to the respective S_0-S_1 absorption bands.

In aliphatic solvents like MCH where hydrogen bonds are particularly strong,[29] the dyes are present as assemblies which can be recognized by the change of the solution color from red

(27) (a) Zhao, D.; Moore, J. S. *Org. Biomol. Chem.* **2003**, *1*, 3471–3491. (b) Zhao, D.; Moore, J. S. *J. Am. Chem. Soc.* **2003**, *125*, 16294–16299.

(28) For publications on sergeants-and-soldiers principle in macromolecules, see: (a) Green, M. M.; Park, J.-W.; Sato, T.; Teramoto, A.; Lifson, S.; Selinger, R. L. B.; Selinger, J. V. *Angew. Chem., Int. Ed.* **1999**, *38*, 3138–3154. (b) Yashima, E.; Maeda, K.; Nishimura, T. *Chem.−Eur. J.* **2004**, *10*, 42–51. For publications on sergeants-and-soldiers principle in supramolecular assemblies, see: (c) Palmans, A. R. A.; Vekemans, J. A. J. M.; Havinga, E. E.; Meijer, E. W. *Angew. Chem., Int. Ed. Engl.* **1997**, *36*, 2648–2651. (d) Wilson, A. J.; van Gestel, J.; Sijbesma, R. P.; Meijer, E. W. *Chem. Commun.* **2006**, 4404–4406. (e) Ajayaghosh, A.; Varghese, R.; George, S. J.; Vijayakumar, C. *Angew. Chem., Int. Ed.* **2006**, *45*, 1141–1144. (f) Ishi-i, T.; Kuwahara, R.; Takata, A.; Jeong, Y.; Sakurai, K.; Mataka, S. *Chem.−Eur. J.* **2006**, *12*, 763–776. (g) Palmans, A. R. A.; Meijer, E. W. *Angew. Chem., Int. Ed.* **2007**, *46*, 8948–8968. (h) Lohr, A.; Würthner, F. *Chem. Commun.* **2008**, 2227–2229.

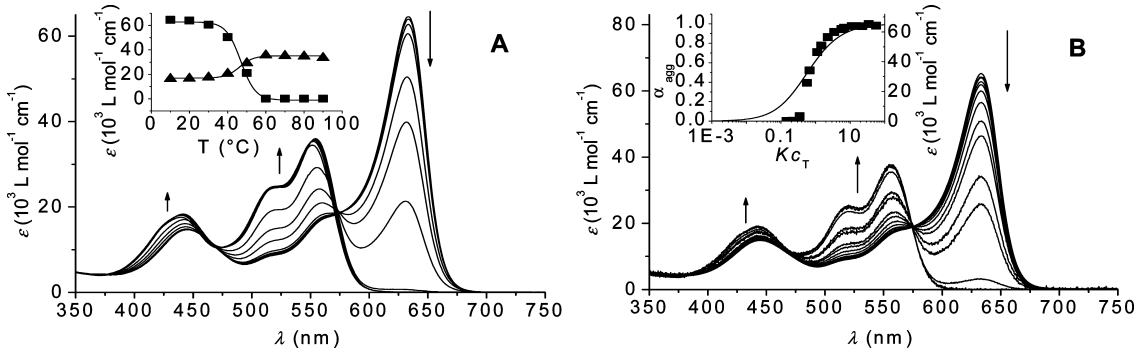

Figure 1. (A) Temperature-dependent UV/vis spectra of **1e** in MCH (1.5×10^{-5} mol L^{-1}) from 10 to 90 °C. Arrows indicate the spectral changes with increasing temperature. (Inset) Change of absorption at 633 nm (■) and 556 nm (▲) upon increasing temperature and calculated lines according to sigmoidal fit. (B) Concentration-dependent absorption spectra of chiral **1e** in MCH ($c = 7.3 \times 10^{-5}$ to 1.9×10^{-7} mol L^{-1}). Arrows indicate the spectral changes with decreasing concentration. (Inset) Change of absorption at 633 nm (■) with decreasing concentration; the curve shows the resulting fit calculated according to isodesmic model.

Table 1. UV/Vis-Absorption Properties of Compounds **1a**−**e** and Reference PBI **2a**

PBI	$\lambda_{abs,mon}$ (nm)[a]	$\varepsilon_{max,mon}$ (L mol^{-1} cm^{-1})[a]	$\varepsilon_{0-0}/\varepsilon_{0-1}$[a]	$\lambda_{abs,agg}$ (nm)[b]	$\varepsilon_{max,agg}$ (L mol^{-1} cm^{-1})[b,c]	$\varepsilon_{0-0}/\varepsilon_{0-1}$[b]
1a[22a]	570	41600	1.55	642	78300	3.78
1b	570	41900	1.55	639	71000	3.33
1c	571	40600	1.54	653	41500	1.39
1d	570	41700	1.57	643	73400	3.74
1e	570	40200	1.56	633	64000	3.25
2a	569	44300	1.59	565	32300	1.26

[a] In CH_2Cl_2. [b] In MCH. [c] Absorption coefficients for the aggregates are given as the values per aggregate-bound monomeric unit.

Table 2. Further Values for Compounds **1a**−**e**[a] and Reference PBI **2a**[b] Obtained from UV/Vis-Absorption Spectra

PBI	T_m (°C)[c]	$fwhm_{mon}$ (cm^{-1})[c,d]	$fwhm_{agg}$ (cm^{-1})[c,e]	$\tilde{\nu}_{agg-mon}$ (cm^{-1})[c]	$\lvert\mu_{eg}\rvert_{mon}$ (D)[c,d]	$\lvert\mu_{eg}\rvert_{agg}$ (D)[c,e]
1a[22a]	59	2550	880	−2510	6.7	8.3
1b	61	2580	910	−2470	6.7	8.1
1c	80	2520	2420	−2760	6.5	7.9
1d	65	2550	900	−2490	6.6	8.1
1e	46	2560	1140	−2330	6.5	8.0
2a	<20[f]	2420	2640	−340	6.8	6.6

[a] $c = 1.5 \times 10^{-5}$ mol L^{-1}. [b] $c = 2.9 \times 10^{-4}$ mol L^{-1}. [c] In MCH. [d] At 90 °C. [e] At 20 °C. [f] At a concentration of 1.5×10^{-5} mol L^{-1} a low degree of aggregation is observed in the accessible temperature range from 10 to 90 °C. At a higher concentration of 10^{-4} mol L^{-1} a melting temperature $T_m = 45$ °C could be determined for compound **2a** (Figure S6, Supporting Information).

(monomer solution) to blue. The absorption spectra of the aggregates in MCH show a strong bathochromic shift of the absorption maxima compared to those of monomers. To get more insights into the aggregation behavior of PBI **1a**−**e**, temperature-dependent UV/vis experiments were performed in MCH at a concentration of 1.5×10^{-5} mol L^{-1}. The spectra for chiral derivative **1e** are shown exemplarily in Figure 1A, and those of **1a**−**d** are given in the Supporting Information (Figures S7−S10). The absorption properties of **1a**−**e** are summarized in Table 1, and further data obtained from absorption spectra are collected in Table 2.

The UV/vis spectra of the aggregates of PBIs **1a**,**b** and **1d**,**e** in MCH at 20 °C show pronouncedly narrowed absorption maximum bands at the maxima with fwhm (full width at half-maximum) values of around 900 cm^{-1}, which is about one-third of the fwhm values (around 2550 cm^{-1}) of the corresponding monomer absorption bands in MCH at 90 °C (Table 2). The absorption coefficients of aggregate solution at λ_{max} are nearly double those observed for the monomers (in CH_2Cl_2 at rt and in MCH at 90 °C, see Table 1). The spectral shift of the absorption maxima of the aggregates is around −2500 cm^{-1} referring to the absorption maxima of the corresponding monomers in the same solvent (see $\tilde{\nu}_{agg-mon}$ values in Table 2). The negative sign of this value indicates the bathochromic shift originated from the geometric arrangement of the monomer units in the aggregates.[24] The ratios of the first and second vibronic bands of the S_0-S_1 transition of the aggregates are more than twice those of the respective monomers.

The absorption spectrum of PBI **1c** aggregate differs from those of **1a**,**b** and **1d**,**e** aggregates insofar as the maximum of the former is not that narrow and the fwhm values for monomeric and aggregate **1e** are very similar. Furthermore, the spectrum of **1c** aggregate shows a more pronounced vibronic fine structure (Figure S3). With a value of 2760 cm^{-1}, the bathochromic shift for **1c** is the largest in this series. For all PBI **1** aggregates, the transition dipole moment μ_{eg} is enhanced to around 8.1 D from approximately 6.6 D for the monomers.[30] At the same concentration no aggregates are formed for reference compound **2a** in MCH and at higher concentration (Figure S6) **2a** self-assembles into dimeric aggregates as our previous study revealed.[22a,31] Since the aggregation of PBIs **1**, except for **1e** (see also nucleation−elongation studies in the discussion part of this work), in MCH is such strong that even at a concentration of 10^{-8} mol L^{-1} aggregates prevail, the aggregation constants for dyes **1a**−**d** could not be determined.

(29) Würthner, F.; Thalacker, C.; Sautter, A.; Schärtl, W.; Ibach, W.; Hollricher, O. *Chem.−Eur. J.* **2000**, *6*, 3871–3885.

Table 3. Emission Properties of Compounds **1a**−**e** and **2a** and Size of the Coherent Domain

	λ_{em} (nm)		Stokes shift (cm^{-1})		Φ_{fl}		τ (ns)		
PBI	mon[a]	agg[b]	mon[a]	agg[b]	mon[a,c,d]	agg[b,c,e]	mon[b,f]	agg[b,g]	N[h]
1a[22a]	602	654	933	286	0.93	0.96	6.8	2.6	2.5
1b	603	655	960	382	0.92	0.53	6.5	2.1	1.6
1c	602	681	902	630	0.94	0.09	5.5−7.1[i]	0.6	1.5−1.6
1d	598	652	821	215	0.94	0.87	7.3	2.6	2.4
1e	600	651	877	437	0.95	0.92	6.6	2.7	2.2
2a	598	n.d.[j]	852	n.d.[j]	0.98	−[k]	7.5	n.d.[j]	−[l]

[a] In CH_2Cl_2. [b] In MCH. [c] Deviation ≤0.03. [d] Determined vs *N,N′*-bis(2,6-diisopropylphenyl)-1,6,7,12-tetraphenoxyperylene-3,4:9,10-tetracarboxylic acid bisimide (Φ_{fl} = 0.96 in $CHCl_3$) using magic angle setup (54.7° between linear polarizers). [e] Determined vs nile blue perchlorate (Φ_{fl} = 0.27 in C_2H_5OH) using magic angle setup. [f] λ_{ex} = 520 nm, λ_{det} = 577−587 nm, at the respective maximum of monomer emission band. [g] λ_{ex} = 520 nm, λ_{det} = 659−695 nm, at the respective maximum of aggregate emission band. [h] Size (number of molecules) of the coherent domain $N = (\tau_{mon}/\tau_{agg}) \times \Phi_{fl,agg}$. [i] Due to the weak signal the deviation is very high. [j] Not determined. [k] No aggregate is formed at concentrations of $\sim 10^{-6}$ mol L^{-1}. [l] Cannot be calculated since $\Phi_{fl,agg}$ is not accessible experimentally.

To compare the aggregation strength of PBIs **1a**−**e**, the "melting" temperature T_m for the transition from aggregates to molecularly dissolved species was determined from temperature-dependent absorption studies in MCH.[32] The absorption versus temperature plots are shown in the insets of Figure 1A and Figures S7−S10, which reveal T_m values of 46−80 °C for PBIs **1a**−**e** (see Table 2).

Due to the weaker aggregation of **1e** in MCH compared to that of **1a**−**d**, it was possible to conduct the concentration-dependent absorption study with **1e** for the whole relevant concentration range. The spectra are shown in Figure 1B that are consistent with the temperature-dependent spectra of the respective aggregate (compare with Figure 1A). However, it was not possible to calculate the binding constant according to the isodesmic model (see inset in Figure 1B) that was usually applied for PBI and other dye assemblies.[15a,d,23d] (See also nucleation−elongation studies in the discussion part of this work.)

The fluorescence spectra of PBI **1a**−**e** monomers and aggregates are mirror images of the respective absorption spectra (see the Supporting Information). The emission maxima for monomeric PBIs **1a**−**e** and **2a** in CH_2Cl_2 are observed at 598−603 nm with high fluorescence quantum yields of 0.92−0.98 which is typical for tetraaryloxy-substituted perylene bisimide chromophores.[16c] With respect to the absorption maxima of the aggregates, their emission maxima are shifted to higher wavelengths exhibiting very small Stokes shifts, which are reduced up to one-third of those of the monomers (see Table 3). For the monomers, lifetimes of 6.5−7.3 ns were obtained, while the aggregates show significantly smaller values of 2.1−2.7 ns for **1a**,**b** and **1d**,**e**, and for **1c** only 0.6 ns.

CD Spectroscopy of Chiral PBI Aggregates. In contrast to **1a**−**d**, the compound **1e** is chiral as it contains 12 alkyl side chains with chirality centers. The solution of monomeric **1e** is CD silent, but the CD spectra of aggregates of **1e** reveal chirality of the assembled system.[33] Negative signals in the ranges of 670−428 nm and 332−253 nm, and positive ones between 428 and 332 nm are observed for **1e** aggregates in MCH (Figure 2). Temperature-dependent CD studies of **1e** in MCH show a decrease of the signal intensity upon increasing temperature and at 70 °C (only monomers are present in the solution) the solution is CD silent.

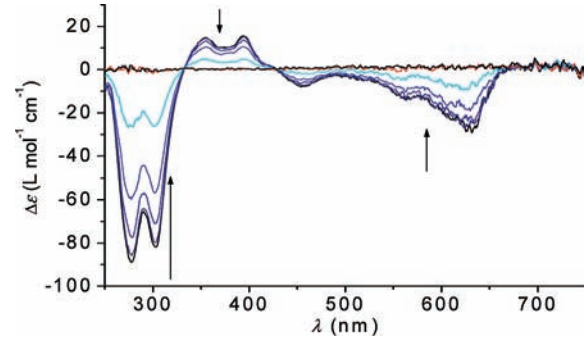

Figure 2. Temperature-dependent CD studies of chiral **1e** in MCH (c = 1.5×10^{-5} mol L^{-1}, 10 to 70 °C). Arrows indicate the spectral changes with increasing temperature.

LD Spectroscopy of 1a Aggregates. To gain insight into the geometric arrangement of the monomeric units within the aggregate in terms of whether the transition dipole moments (polarized along the N−N axis) of the monomers are arranged rather perpendicular or parallel to the aggregate direction, LD measurements were performed. In contrast to CD spectroscopy, where the sample is unoriented, for LD spectroscopy it is essential that the sample is oriented during the measurement. This can be achieved, e.g., by incorporation of molecular aggregates in polymer films, which are then stretched in one direction,[34] or by orienting the sample in a flow cell by rotating a quartz rod placed in the middle of the cuvette to get a uniform flow in horizontal direction in which long molecular aggregates are oriented.[35] We have applied the latter technique for **1a** aggregates in MCH solution. For LD measurements, the probe was irradiated by linear polarized light parallel and perpendicular to the orientation axis, and the detected signals were subtracted from each other.[36] A positive LD signal in the range of 477−675 nm and a negative one in the range of 395−477 nm were observed for **1a** aggregates in MCH (Figure 3).

(30) Transition dipole moments were calculated according to literature: Liptay, W.; Wortmann, R.; Schaffrin, H.; Burkhard, O.; Reitinger, W.; Detzer, N. *Chem. Phys.* **1988**, *120*, 429–438. The molar absorption coefficients and the transition dipole moments for the aggregates are given per aggregate-bound monomeric units.

(31) Chen, Z.; Baumeister, U.; Tschierske, C.; Würthner, F. *Chem.−Eur. J.* **2007**, *13*, 450–465.

(32) (a) Apperloo, J. J.; Janssen, R. A. J.; Malenfant, P. R. L.; Fréchet, J. M. J. *Macromolecules* **2000**, *33*, 7038–7043. (b) Schenning, A. P. H. J.; Jonkheijm, P.; Peeters, E.; Meijer, E. W. *J. Am. Chem. Soc.* **2001**, *123*, 409–416.

(33) Note that for the present aggregates no LD signal was observed for unoriented samples; thus, a contribution of LD to the CD spectra of these assemblies can be excluded.

(34) Holmén, A.; Broo, A.; Albinsson, B.; Nordén, B. *J. Am. Chem. Soc.* **1997**, *119*, 12240–12250.

(35) Dafforn, T. R.; Rajendra, J.; Halsall, D. J.; Serpell, L. C.; Rodger, A. *Biophys. J.* **2004**, *86*, 404–410.

(36) Rodger, A.; Nordén, B. *Circular Dichroism and Linear Dichroism*; Oxford University Press: Oxford, 1997.

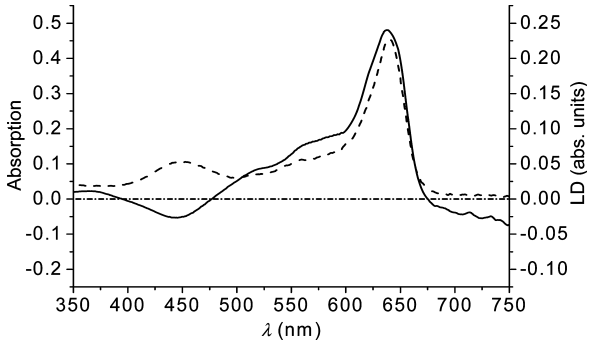

Figure 3. Absorption (− − −) and LD (—) spectra of **1a** in MCH ($c = 10^{-4}$ mol L^{-1}) measured in a flow cell setup. The absorption spectrum was recorded under unoriented conditions.

Sergeants-and-Soldiers Studies. We have studied the coaggregation behavior of chiral PBI **1e** and achiral **1d** by CD spectroscopy for different ratios of these dyes to explore if the sergeants-and-soldiers principle applies for these PBI aggregates. For this purpose, the stock solutions of **1d** and **1e** in MCH were mixed in different ratios and equilibrated at 25 °C prior to measurements.[37] The CD spectra in Figure 4A show that the $\Delta\varepsilon$ values increase with increasing mole amount of **1e** in mixtures. For better illustration of the change of chiral bias for the heteroaggregate, the anisotropy factor $g = \Delta\varepsilon/\varepsilon$ was calculated and is plotted vs the mole fraction χ_{1e} of chiral **1e**, revealing a nonlinear correlation (Figure 4B). To explore the kinetics of intermixing of the two original aggregates, solutions of **1e** and **1d** were mixed in different ratios at room temperature, and the time-dependent change of the intensity of the CD signals (spectra not shown) at 303 nm was recorded, and the g values are plotted against time (Figure 4C). It was observed that the g value increases strongly with time at the beginning and, depending on the amount of chiral **1e**, reaches different maxima at different times. Since the aggregate melting temperatures (T_m) for **1e** and **1d** are quite different (46 and 65 °C, respectively), the change of T_m for equilibrated mixtures of different ratios of these aggregates has been investigated as well, and the melting temperatures estimated from temperature-dependent absorption spectroscopy are plotted vs the mole fraction of chiral **1e** (Figure 4D) which shows a linear relationship.

Microscopic Studies. We have investigated the aggregates of present PBIs by atomic force microscopy (AFM) on highly oriented pyrolytic graphite (HOPG) and silicon wafer. AFM images of **1a** aggregates on HOPG show monolayers consisting of parallel aligned rows of a few hundred nanometers in length (Figure 5A,B). The height of these monolayers was estimated to be 0.3 ± 0.1 nm, and the periodic distance of the rows, which corresponds to the width, was estimated as 5.7 ± 0.2 nm. Some parts of the monolayers are aligned with an angle of 60° to each other (see Figure 5B). Upon spin-coating of aggregate solutions of PBIs **1a**−**e** onto silicon wafers, interwoven networks were observed by AFM (the image of **1d** is shown in Figure 5C and those for **1a**−**c** and **1e** in Figure S13, Supporting Information). These consist of thin fibrillar assemblies, which were found to be more frequently interlinked with each other for probes obtained from more highly concentrated solutions. The molecular dimensions of the assemblies were estimated by cross-section analysis, and the data are collected in Table 4. The height values are in the range of 1.9−2.5 nm, while the width values are found to be 7.2−8.6 nm. Except for aggregates of **1c**, a top-to-top periodicity along the fibers was observed that can be attributed to the existence of helical arrangement. The values for the helical pitches (the top-to-top periodicity corresponds to the half of a helical pitch) were estimated to be around 13.0−15.4 nm with strong variation within one fiber. In the absence of higher-resolution AFM images due to the limitation of the tip size, it is uncertain whether left- or right-handed helical aggregates or a mixture of both are present. For the same reason, the handedness in mixed aggregates of **1e** and **1d** (3:7) cannot be deduced from the AFM image (Figure 5F).

For better visualization of the monolayer coverage on HOPG (Figure 5A,B), scanning tunneling microscopy (STM) measurements were performed. The aggregates of **1a** were spin-coated onto HOPG from MCH solution, and a small amount of phenyloctane was dropped onto the probe to conduct the STM measurements (Figure 6). Monolayers consisting of parallel aligned rows were observed with parts that are oriented with an angle of 60° with respect to the others, which is in agreement with the observations of AFM studies. The width of these rows was determined to be 3.9 ± 0.2 nm. In contrast to the AFM studies, a fine structure within the rows could be visualized by STM. The bright areas are attributed to more conducting, i.e., extended aromatic parts (perylene core) of the assemblies. A distance of these bright areas in the direction of the rows was measured to be 1.6 ± 0.2 nm obtained from cross-section analysis.

Discussion

Aggregate Structure Model. In our previous communication,[22a] we have suggested a model for the aggregate structure of PBI **1a** assemblies. The results of our present detailed studies with an extended series of PBIs **1a**−**e** now underpin this model; furthermore, valuable mechanistic insights into the aggregation process of these PBIs are obtained (a schematic representation of the model is illustrated in Figure 7). AFM measurements of PBI **1a** aggregates on silicon wafers revealed helical strands (both left- and right-handed),[22a] while monolayers could be observed on HOPG surfaces (Figure 5A,B) owing to the template effect of this substrate. The observed lamellae structures for **1a** aggregates on HOPG by STM (Figure 6) indicate hydrogen-bonded chains of perylene bisimides (discussed later in detail). Already previously we could provide evidence for hydrogen-bond formation between imide groups of PBI **1a** molecules by FT-IR spectroscopy and ^{1}H NMR measurements at different concentrations.[22a] The UV/vis spectroscopic studies revealed a large bathochromic shift for the absorption band of the S_0-S_1 transition of the aggregates of PBIs **1a**−**e** compared to that of the respective monomeric dyes (Figure 1 and Figures S7−S10, Supporting Information). Such pronounced bathochromic shifts cannot be rationalized solely in terms of hydrogen-bonded perylene bisimide chains, but can arise only from closely stacked π-systems. According to Kasha's exciton model,[24] this spectral feature further implies that the monomer units are stacked in a slipped fashion (slip angle $<54.7°$, see Spectroscopic Studies section below). Furthermore, previous studies of the fluorescence anisotropy[22a] and the present results of CD investigations (helical aggregate formation, illustrated in Figure 7C) strongly suggest a rather parallel alignment of

(37) The measurements were repeated after several hours (up to 150 h) at 25 °C until no significant change in $\Delta\varepsilon$ was obtained.

(38) *Disco Very Studio ViewerPro*; Accelrys Inc.: San Diego, CA, 2002; www.accelrys.com.

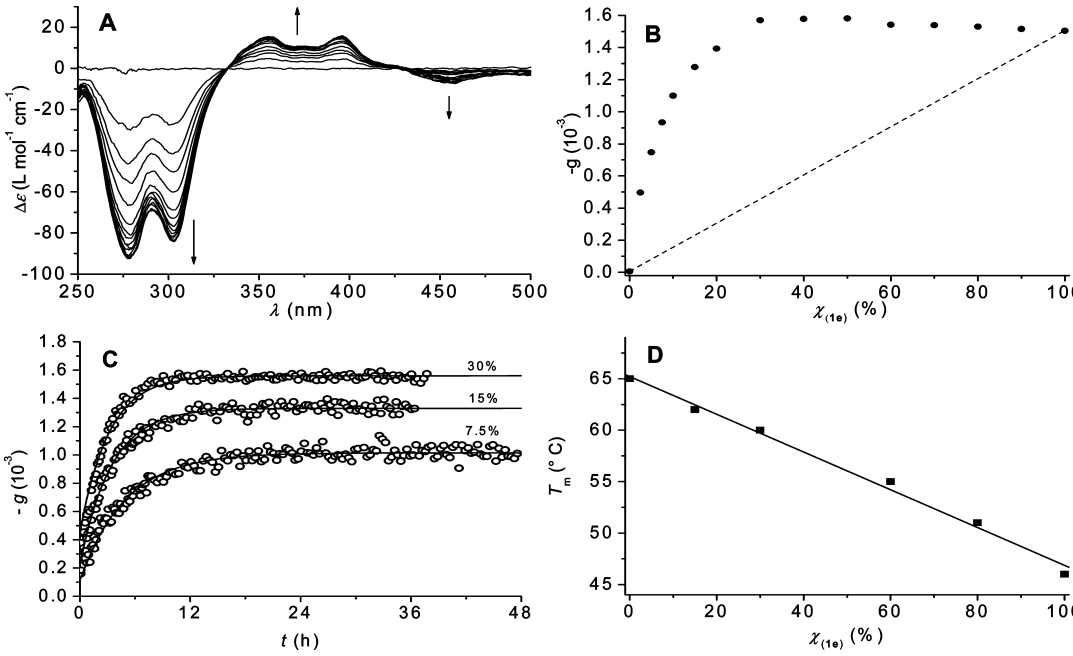

Figure 4. (A) CD spectra of mixtures of J-aggregates of **1d** and **1e** in MCH ($c_{tot} = 1.5 \times 10^{-5}$ mol L^{-1}) with variation of mole fraction $\chi_{(1e)}$ of chiral **1e**. Arrows indicate increasing mole fraction $\chi_{(1e)}$. (B) Dependence of the anisotropy factor g at 303 nm on the mole fraction $\chi_{(1e)}$ of chiral **1e** as obtained from CD spectra in (A). The dashed line in (B) represents the expected g values in the absence of any chiral amplification. (C) Time-dependent anisotropy factors g at 303 nm of intermixed J-aggregates of **1d** and **1e** with various mole fractions of chiral **1e** (7.5 to 30% **1e**) in MCH ($c = 1.5 \times 10^{-5}$ mol L^{-1}) at 25 °C. The two different aggregate solutions were mixed at $t = 0$. The solid lines present the exponential curve fits (details are given in the Supporting Information). (D) Dependence of the aggregate melting temperature T_m on the mole fraction $\chi_{(1e)}$ of chiral **1e** of thermodynamically equilibrated mixtures of J-aggregates of **1d** and **1e** in MCH ($c_{tot} = 1.5 \times 10^{-5}$ mol L^{-1}): experimental data points (■) and linear fit (solid line).

the S_0–S_1 transition dipole moments of the monomeric units with respect to the aggregate direction (illustrated in Figure 7C,D), which is in congruity with the LD results. Comparison of the aggregation behavior of PBIs **1** with that of reference PBI **2a** reveals that the latter forms only dimers and at considerably higher concentrations,[22a] and the results of present cooperative growth studies indicate the formation of a nucleus prior to elongation of the aggregate in a dynamic process (Figure 7B). Taking into account all of these experimental results, the arrangement of the monomer units in aggregates was explored by molecular modeling (see next section). The structural parameters obtained by molecular modeling were then used to estimate the exciton coupling between the closely packed neighboring dyes according to Kasha's model and compared with the observed spectral shifts in the UV/vis absorption spectra (see Spectroscopic Studies section below), which are in good agreement, confirming the viability of the proposed model.

Molecular Modeling. In order to gain insight into the structural details of helical strands, molecular modeling was performed. Perylene bisimides with oxygen atoms at the bay positions (aryl substituents are omitted for calculations) were assembled using HyperChem Professional 7.03 for Windows.[39] The monomers were preoptimized with MM+ force field calculations, and thereafter the geometry optimizations *via* short molecular dynamic simulations were carried out with AMBER.[40] All atoms in supramolecular structures were free to move in each equilibration.

Since *M* and *P* conformers of tetraaryloxy perylene bismides exist in equal amounts (racemate), both atropisomers were taken into account for molecular modeling, but only assemblies of one conformer arrange in helical structure with particular handedness (*M* conformers build up left-handed and *P* conformers right-handed helical strands).

Simulations were done on double-string arrangement of (*M*)-configured perylene bisimides, and excellent agreement with the experimental results was obtained. The half of the helical pitch is calculated as $p/2 = 6$ nm (Figure 5G), which corresponds nicely to the periodic top-to-top length of the helical structure (around 6.5−7.7 nm) obtained from AFM images (see Figure 5E and Table 4). From geometrical considerations, including the results of AFM and STM investigations, it can be concluded that this half of one pitch is constructed by eight to ten molecules within the double string.

The width of the strands depends on the molecular width (perpendicular to the N−N axis) of one monomeric PBI which was calculated by MM3 method as 3.0, 4.4, and 5.7 nm for PBIs without, with C_8- and C_{12}-alkyl chains, respectively. This again is in excellent agreement with the experimental results of AFM measurements (Table 4).

Furthermore, values for the distance between chromophore centers in $\pi-\pi$-stack direction ($r_\pi = 7.8$ Å) and in hydrogen-bond direction ($r_H = 14.1$ Å) as well as for the corresponding slip angles θ that result from the translational offset of two parallel-arranged molecules ($\theta_\pi = 28.1°$ and $\theta_H = 9.9°$), could be obtained from molecular modeling studies (for definition of the distances and angles see also Figure 7D and Figure S14B, Supporting Information). These values of the geometrical arrangement of the monomers in the assemblies are used to calculate the spectral shift by Kasha's exciton theory[24] (see next section).

(39) *HyperChem Professional 7.03*; Hypercube, Inc.: Gainesville, FL, 2002.
(40) Weiner, S. J.; Kollman, P. A.; Nguyen, D. T.; Case, D. A. *J. Comput. Chem.* **1986**, *7*, 230–252.

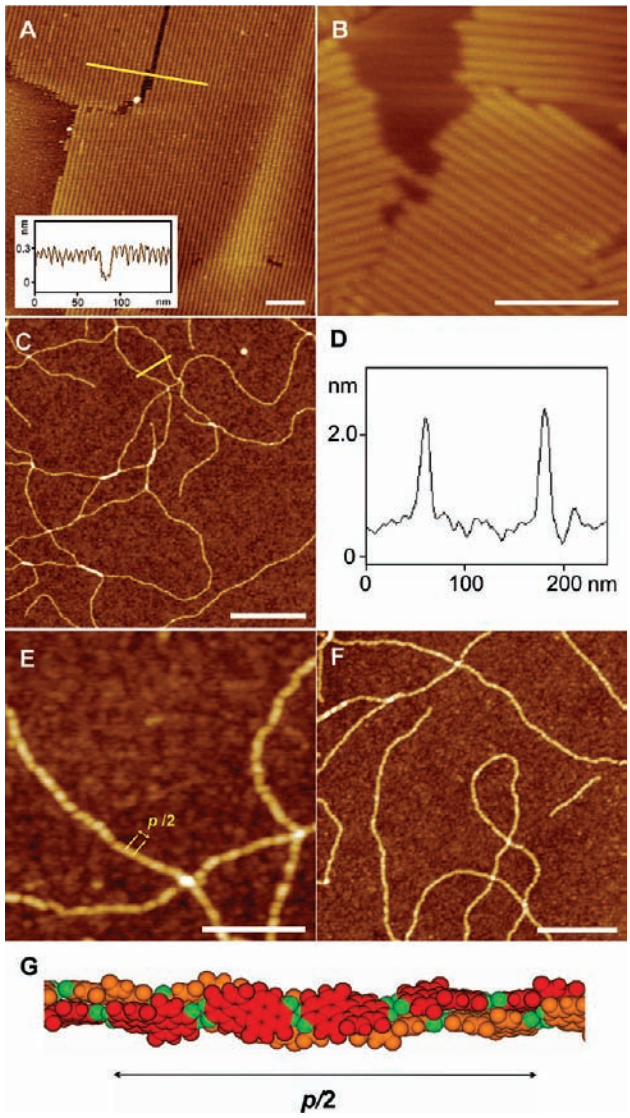

Figure 5. Tapping-mode height AFM images of (A, B) perylene bisimide **1a** monolayers adsorbed on basal plane of HOPG by spin-coating (4000 rpm) from MCH solution ($c = 6 \times 10^{-5}$ mol L^{-1}). [Inset in (A)] Cross-section analysis provided an average height value of 0.3 ± 0.1 nm and a width of 5.7 ± 0.2 nm for the aligned rows. AFM studies with solutions of perylene bisimide **1a** in toluene and CCl_4 provided similar results (images are not shown). (C, E) Self-assemblies of **1d** spin-coated (2000 rpm) onto silicon wafers from MCH solutions ($c = 5 \times 10^{-6}$ mol L^{-1}). (D) Cross-section analysis along the yellow line in (C) provided a height value of 2.0 ± 0.2 nm for PBI **1d** assemblies. In image (E) the periodic top-to-top length (corresponding to the half-pitch *p*/2; measured as 6.9 ± 2.0 nm) could be visualized. (F) AFM height image of 3:7 intermixed aggregates of **1e** and **1d** spin-coated onto silicon wafers from solution in MCH ($c = 7 \times 10^{-6}$ mol L^{-1}). The scale bars and *z* scales are (A): 45 and 1.5 nm, (B): 45 and 2.0 nm (C): 300 and 5 nm, (E): 100 and 5 nm, (F): 200 and 5 nm, respectively. (G) Molecular model (HyperChem Release 7.03 for Windows, AMBER force field) for the supramolecular structure of perylene bisimide **1** aggregates. The half of a helical pitch *p*/2 was calculated as 6 nm. For this graphic, Accelrys DS ViewerPro 5.0 was used.[38] Perylene cores including oxygens at bay positions and free carbonyl oxygens are shown in red or orange, and hydrogen-bonded carbonyl oxygens and imide hydrogens are shown in green. Phenoxy substituents are omitted for clarity.

Spectroscopic Studies. The observed strongly bathochromically shifted absorption bands of the aggregates of PBIs **1a**−**e** can be explained by Kasha's theory, which is an approximation, based on the assumption that the transition dipole moments of the monomers are point dipoles.[24] The distance of the monomeric units plays an important role for the spectral shift as well as the angle of the center of one monomer to the center of the adjacent monomer and to the aggregate direction (see also Figure S14, Supporting Information). For short distances and small angles (close to 0°), the spectral shift is strongly bathochromic (J-aggregate), while for short distances and large angles (close to 90°) it is strongly hypsochromic (H-aggregate), and for large distances or angles around 54.7° the spectral shifts are rather small.[24] This implies that in present assemblies, for which strongly bathochromic shifted J-bands are observed, the monomers are quite closely packed with short distances to each other and the slip angle resulting from the translational offset of the monomers is small.

Under the premise that only nearest neighbors interact in an aggregate composed of a sufficiently large number of mol-

Table 4. Dimensions of PBI **1a**−**e** Aggregates Spin-Coated onto Silicon Wafers from MCH Solutions Determined by AFM Measurements

PBI	height (nm)	width (nm)	pitch (nm)
1a[a]	2.0 ± 0.2	8.4 ± 2.6	13.0 ± 3.4
1b	1.9 ± 0.2	8.2 ± 2.5	13.5 ± 2.5
1c	2.5 ± 0.3	7.2 ± 2.5	—[b]
calcd	3.0[c]	5.7[c]	12.0[d]
1d	2.0 ± 0.2	8.2 ± 1.7	13.8 ±4.0
1e	2.2 ± 0.4	8.6 ± 3.0	15.0 ±4.0
1e/1d (30:70)	2.0 ± 0.3	8.1 ± 1.5	15.4 ± 3.8
calcd	3.0[c]	4.8[c]	12.0[d]

[a] The values are taken from ref 22a and shown for completeness. [b] No pitch could be resolved. [c] Obtained from MM3 calculations. [d] Obtained from AMBER force field calculations.

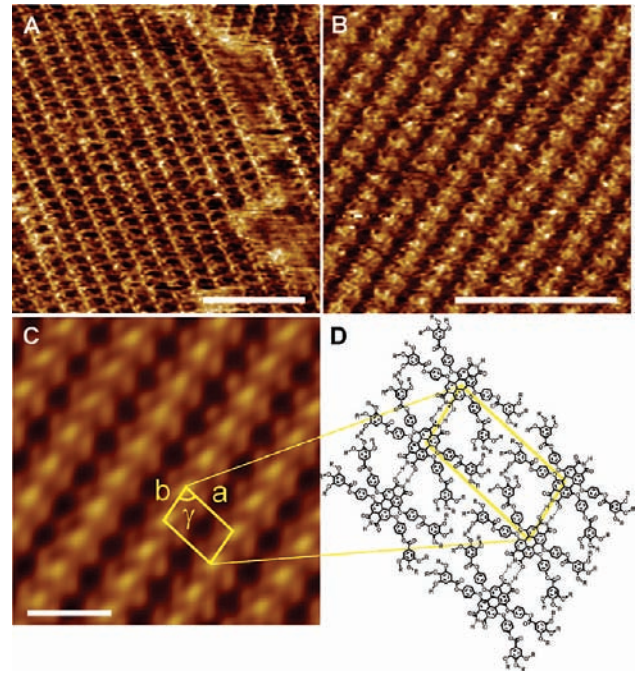

Figure 6. STM images of perylene bisimide **1a** aggregates on the basal plane of HOPG spin-coated (4000 rpm) from MCH solution ($c = 6 \times 10^{-5}$ mol L^{-1}). Tunneling parameters: (A) $I = 1.32$ pA, $U = -0.87$ V; (B) $I = 1.0$ pA, $U = -1.20$ V. Scale bars are 20 nm, *z* scale: 0.7 nm. Image (C) is a zoomed and filtered section of image (B). Scale bar is 5 nm. (D) Schematic illustration of the molecular arrangement of PBI **1a** ($R = C_{12}H_{25}$) on HOPG. Unit cell parameters *a*, *b*, and γ are 3.9 ± 0.2 nm, 1.6 ± 0.2 nm, and 72 ± 5°, respectively.

ecules,[41] the transition energy for the aggregate species ΔE_{agg} can be expressed as

$$\Delta E_{agg} = \Delta E_{mon} + \Delta E_{vdW} + \sum_i J_i \quad (1)$$

where ΔE_{mon} is the transition energy for the isolated monomer, ΔE_{vdW} the difference in van-der-Waals interaction energy between excited- and ground-state units of two adjacent molecules, and J_i is the exciton splitting for one interaction of two adjacent molecules. The latter can be calculated for parallel-arranged molecules according to eq 2,[24,42]

$$J_i = \frac{|\mu_{eg}|^2}{4\pi\varepsilon_0 r_i^3}(1 - 3\cos^2\theta_i) \quad (2)$$

where μ_{eg} is the transition dipole moment of the monomer, ε_0 the permittivity of vacuum, r_i the distance between the centers of two adjacent molecules (with $i = \pi$, H; π: in $\pi-\pi$-stack direction, and H: in H-bond direction; for definition of the distances and angles see also Figure 7D and Figure S14B, Supporting Information), and θ_i the slip angle that results from the translational offset of these two parallel-arranged molecules (where the transition dipole moments are arranged parallel as well).

On the basis of the above-mentioned assumptions and the fact that ΔE_{vdW}, which cannot be determined experimentally, is negative, one can approximate the spectral shift $\Delta\tilde{\nu}_{agg-mon}$ of the aggregate band (wavenumber $\tilde{\nu}_{agg}$) with respect to the monomer band (wavenumber $\tilde{\nu}_{mon}$) as

$$\Delta\tilde{\nu}_{agg-mon} < \frac{\sum_i J_i}{hc} = m\frac{J_\pi}{hc} + n\frac{J_H}{hc} \quad (3)$$

The left term of eq 3 can be determined experimentally and the right term can be calculated for m and n nearest neighbors in the respective direction with h being the Planck's constant and c the speed of light. For a step by step derivation of eq 3 and calculation of $|\mu_{eg}|$, see the Supporting Information.

For aggregates of **1a**, the calculated values for $J_\pi/hc = -635$ cm^{-1} and $J_H/hc = -154$ cm^{-1} provide an estimated spectral shift of $\Delta\tilde{\nu}_{agg-mon} < -1578$ cm^{-1} for the double string cable model ($m = 2$, $n = 2$), which is in good agreement with the experimental data ($\Delta\tilde{\nu}_{exp} = -2510$ cm^{-1}). The difference of the calculated value compared with the experimental one can be attributed to the approximations of Kasha's theory and the lack of the knowledge of van-der-Waals interaction energy in this system. Similar results were obtained for the assemblies of PBI **1b**−**e**, assuming the same geometric arrangements of the monomeric units as for that of **1a**.[43]

Furthermore, the increased ratio of the first and the second vibronic of the S_0-S_1 transition of the aggregate compared to that of the monomers shows that the transition to the first vibronic energy level of the S_1 state ($S_{0(v=0)} \rightarrow S_{1(v=0)}$) possesses most of the oscillator strength, which is typical for J-aggregates.[44] Likewise, the increase of the transition dipole moment for aggregates of PBIs **1a**−**e** compared with that of the respective monomer (for data see Table 2) can be attributed to an enhancement of the oscillator strength in the aggregates. Temperature-dependent absorption studies of the present aggregates revealed a variation of T_m from 46−80 °C. Since T_m reflects the aggregation strength by comparing assemblies under identical conditions, the weakest aggregate is formed by PBI **1e** (revealing the lowest T_m value), bearing the shortest, branched alkyl chains of the present PBIs (for a more extended discussion, see the Supporting Information) which is also reflected in the fact that no aggregates of PBI **1e** are formed at low concentrations ($<10^{-7}$ mol L^{-1}), in contrast to the assemblies of PBIs **1a**−**d**.

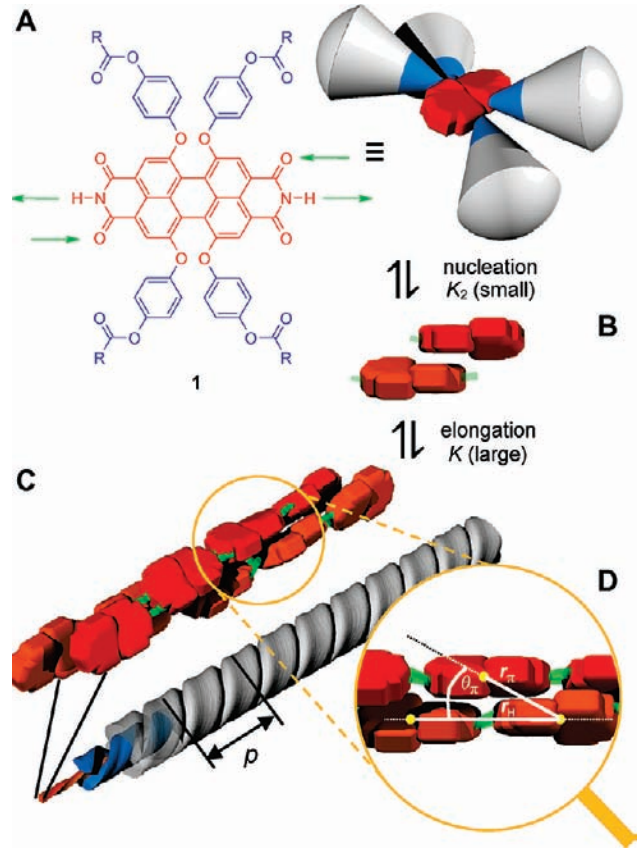

Figure 7. Schematic illustration of self-assembly of the perylene bisimide dyes **1** into J-type aggregates. (A) Molecular structures of **1** (substituents R are defined in Chart 1) and graphical representation of the monomer. (B) Schematic representation of π-stacked dimeric nucleus and (C) that of an extended hydrogen-bonded aggregate of **1**: red (and orange) twisted blocks represent the perylene bisimide core (in the adjacent chain), gray cones with a blue apex represent the bay substituents, and green lines represent hydrogen bonds. The dyes **1** self-assemble in a helical fashion as shown in the magnification (substituents have been omitted and only the left-handed helical structure is shown for simplicity). (D) The magnifier visualizes the J-type arrangement of the core perylene bisimide units in a double string cable in the side view, and the distances and angle are defined: r_π and r_H represent the distances between the centers (yellow dots) of two adjacent molecules in $\pi-\pi$-stack and in H-bond direction, respectively; the slip angles θ_π and θ_H (for definition see Figure S14, Supporting Information), resulting from the longitudinal (θ_π) and translational (θ_H) offset, represent the angle between the aggregation direction and the direction from the center of one molecule to the center of the adjacent one in $\pi-\pi$-stack (θ_π) and in H-bond (θ_H) direction, respectively.

(41) Evans, C. E.; Song, Q.; Bohn, P. W. *J. Phys. Chem.* **1993**, *97*, 12302–12308.
(42) Würthner, F.; Yao, S.; Debaerdemaeker, T.; Wortmann, R. *J. Am. Chem. Soc.* **2002**, *124*, 9431–9447.
(43) The calculated values are for **1b**:−1578 cm^{-1}, **1c**:−1486 cm^{-1}, **1d**: −1534 cm^{-1}, and **1e**: −1486 cm^{-1}; experimental values are given in Table 2. The variation of these calculated values results from the slightly different values of the respective monomer transition dipole moments.
(44) The oscillator strength is distributed over many levels in the exciton band, but the lowest one contains most of the oscillator strength: Davydov, A. S. *Theory of Molecular Excitons*; Plenum Press: New York, 1971.

For the aggregates of PBI **1a**−**e**, smaller Stokes shifts compared to those of the monomers were observed (see Table 3) that can be ascribed to conformationally more uniform dye molecules in the more rigid aggregate environment. It was noticed that the aggregates of PBIs **1a** and **1d**,**e** bearing 12 alkoxy chains per monomeric unit exhibit very high fluorescence quantum yields, whereas for the aggregates of PBIs with only eight alkoxy chains, particularly for PBI **1c**, the fluorescence quantum yield decreases drastically. Similar differences were observed for fluorescence lifetimes as for the aggregate of **1c** the shortest lifetime in this series was detected (Table 3). This fluorescence quenching as well as the observed differences in the aggregate absorption spectrum of PBI **1c** compared to those of the other PBIs **1a**,**b** and **1d**,**e** might be due to the less dense alkyl shell that cannot completely wrap the π-stacked double cable aggregate in the case of **1c**. With the knowledge of the fluorescence quantum yield of the aggregate Φ_{agg} and the fluorescence lifetimes of the aggregate τ_{agg} and the respective monomer τ_{mon}, the size of the coherent domain N in the assembly can be estimated according to the eq 4:[45]

$$N \times \tau_{agg} = \Phi_{agg} \times \tau_{mon} \quad (4)$$

By applying the fluorescence data (given in Table 3) in eq 4 the size of the coherent domain in assemblies of PBIs **1a**−**e** was estimated to be two to three PBI molecules at room temperature.

Nucleation−Elongation Mechanism. In solution, aggregate formation can be ascribed to chemical equilibria between monomeric and aggregated species. If there are more than two aggregated species, multiple equilibria may exist in the system. The simplest model to describe extended dye aggregates is the isodesmic model.[46,47] In this model it is assumed that the aggregates are one-dimensional. All equilibrium constants or Gibbs free energy changes are equal for all binding events (addition of one monomer to another or to an aggregated species, i.e., $K_2 = K_3 = K_4 \ldots = K_i \ldots = K$). Mathematically this model can be described as a quadratic function of α_{mon} and can be expressed as follows:

$$\alpha_{agg} = 1 - \alpha_{mon} = 1 - \frac{c_{mon}}{c_T} = 1 - \frac{2Kc_T + 1 - \sqrt{4Kc_T + 1}}{2(Kc_T)^2} \quad (5)$$

where α_{mon} and α_{agg} are the molar fraction of the monomeric and aggregated species, respectively, c_{mon} and c_T are the concentrations of monomeric species in solution and of all dyes in the system, respectively, and K is the equilibrium constant. By applying eq 6, this mathematical expression can be connected to absorption spectra leading to eq 7:

$$\alpha_{agg} = 1 - \frac{\varepsilon(c_T) - \varepsilon_{agg}}{\varepsilon_{mon} - \varepsilon_{agg}} \quad (6)$$

$$\varepsilon(c_T) = \frac{2Kc_T + 1 - \sqrt{4Kc_T + 1}}{2(Kc_T)^2}(\varepsilon_{mon} - \varepsilon_{agg}) + \varepsilon_{agg} \quad (7)$$

where ε_{mon}, ε_{agg}, and $\varepsilon(c_T)$ are the molar absorption coefficients of free monomeric dyes, aggregated dyes, and the concentration c_T, respectively. Usually PBI dye aggregates can be described very well by the isodesmic model (as they are of one-dimensional nature).[15a,d,23d,48] However, as described in the Results section, this model is not applicable to J-aggregates of **1e** (see inset in Figure 1B) since concentration-dependent absorption data could not be fitted by eq 7. The abrupt increase in absorption at 633 nm at a certain "critical" concentration of PBI **1e** (inset in Figure 1B) suggests a non-isodesmic aggregation process in which two noncovalent interactions, i.e., $\pi-\pi$ stacking and hydrogen bonding, cooperate favorably to initiate aggregate growth at a defined concentration. Thus, the nucleation−elongation model[27a,49] can be applied to this system. Note that, to the best of our knowledge, this model has not been applied so far to concentration-dependent UV/vis studies of synthetic assemblies,[50] but for biomacromolecules.[51] In the cooperative nucleation−growth model it is assumed that the equilibrium constant for the formation of the nucleation (K_{nuc}) is smaller than that of the elongation (K). The simplest version of this model has only one dimerization step of nucleation, followed by isodesmic elongation steps. This means, only the dimerzation (with equilibrium constant K_2) differs energetically relative to the following steps ($K_2 \neq K_3 = K_4 \ldots = K_i \ldots = K$), implying a nucleus size of 2 (see also Figure 7B for graphical illustration). This relation can be mathematically described as a cubic function presented in eq 8:

$$\alpha_{mon}^3(Kc_T)^2(\sigma - 1) + \alpha_{mon}^2 Kc_T(Kc_T - 2(\sigma - 1)) - \alpha_{mon}(2Kc_T + 1) + 1 = 0 \quad (8)$$

for a nucleus consisting of a dimer and $\sigma = K_2/K$. Even though it is not possible to solve eq 8 for α_{mon} as a function of Kc_T for general cases, one can easily calculate Kc_T as a function of Kc_{mon} for certain σ values by using eq 9. The

(45) A coherent size N of 3−4 molecules was estimated by an alternative approach using the fwhm values of the corresponding 0−0 vibronic transitions according to the equation $fwhm_{mon}/fwhm_{agg} = \sqrt{N}$ (Busse, G.; Frederichs, B.; Petrov, N. K.; Techert, S. *Phys. Chem. Chem. Phys.* **2004**, *6*, 3309−3314).

(46) The isodesmic model is also called multistage open association, ladder-association, free-association, or equal K model.

(47) (a) Martin, R. B. *Chem. Rev.* **1996**, *96*, 3043–3064. (b) CiferriA. In *Supramolecular Polymers*; Ciferri, A., Eds.; CRC Press: Boca Raton, 2005; pp 29−75. (c) Baxter, N. J.; Williamson, M. P.; Lilley, T. H.; Haslan, E. *J. Chem. Soc. Faraday Trans. 2* **1996**, *92*, 231–234. (d) van der Schoot, P.; Michels, M. A. J.; Brunsveld, L.; Sijbesma, R. P.; Ramzi, A. *Langmuir* **2000**, *16*, 10076–10083. (e) Henderson, J. R. *J. Chem. Phys.* **2000**, *113*, 5965–5970. (f) Chen, Z.; Lohr, A.; Saha-Möller, C. R.; Würthner, F. *Chem. Soc. Rev.* **2009**, *38*, 564–584, and reference 27a.

(48) van Herrikhuyzen, J.; Syamakumari, A.; Schenning, A. P. H. J.; Meijer, E. W. *J. Am. Chem. Soc.* **2004**, *126*, 10021–10027.

(49) The model of nucleation and elongation is also called nucleated self-assembly, nucleation-growth, or initiation−elongation model.

(50) For some other applications of nucleation−elongation model to synthetic self-assemblies, see: (a) Jadzyn, J.; Stockhausen, M.; Zywucki, B. *J. Phys. Chem.* **1987**, *91*, 754–757. (b) Lortie, F.; Boileau, S.; Bouteiller, L. *Chem.−Eur. J.* **2003**, *9*, 3008–3014. (c) Simic, V.; Bouteiller, L.; Jalabert, M. *J. Am. Chem. Soc.* **2003**, *125*, 13148–13154. (d) Percec, V.; Unger, G.; Peterca, M. *Science* **2006**, *313*, 55–56. (e) Jonkheihm, P.; van der Schoot, P.; Schenning, A. P. H. J.; Meijer, E. W. *Science* **2006**, *313*, 80–83. (f) Smulders, M. M. J.; Schenning, A. P. H. J.; Meijer, E. W. *J. Am. Chem. Soc.* **2008**, *130*, 606–611, and 4204.

(51) Concentration-dependent absorption studies of bacteriochlorophyl *a*, see: (a) Fisher, J. R. E.; Rosenbach-Belkin, V.; Scherz, A. *Biophys. J.* **1990**, *58*, 461–470. For some further applications of the nucleation−elongation model to peptides and proteins, see reference 25. (b) Attri, A. K.; Lewis, M. S.; Korn, E. D. *J. Biol. Chem.* **1991**, *266*, 6815–6824. (c) Niranjan, P. S.; Yim, P. B.; Forbes, J. G.; Greer, S. C.; Dudowicz, J.; Freed, K. F.; Douglas, J. F. *J. Chem. Phys.* **2003**, *119*, 4070–4084. (d) Chen, Y.; Bjornson, K.; Redick, S. D.; Erickson, H. P. *Biophys. J.* **2005**, *88*, 505–514. For concentration-dependent absorption studies of bacteriochlorophyl *c*,*d*, see: (e) Balaban, T. S.; Leitich, J.; Holzwarth, A. R.; Schaffner, K. *J. Phys. Chem. B* **2000**, *104*, 1362–1372. (f) Balaban, T. S.; Tamiaki, H.; Holzwarth, A. R. *Top. Curr. Chem.* **2005**, *258*, 1–38. (g) Huber, V.; Sengupta, S.; Würthner, F. *Chem.−Eur. J.* **2008**, *14*, 7791–7807.

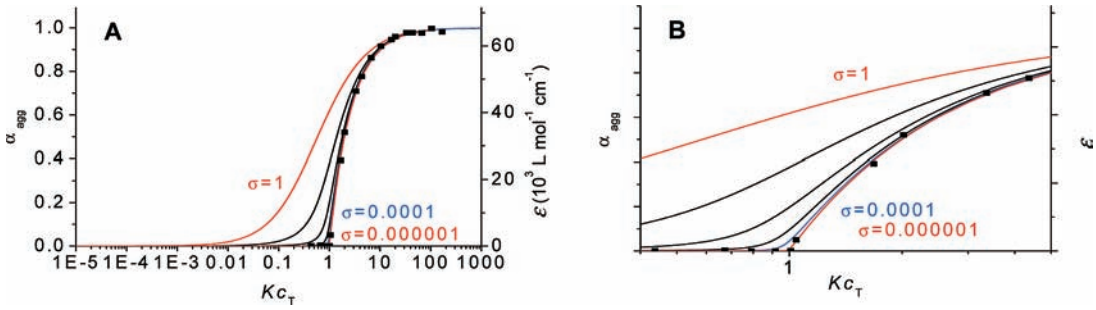

Figure 8. (A) Fraction of aggregated molecules α_{agg} plotted as a function of Kc_T with different σ values according to cooperative nucleation−elongation model (lines from left to right: σ = 1, 0.1, 0.01, 0.001, 0.0001, and 0.000001), and plot of experimental absorption data of chiral **1e** in MCH ($c = 7.3 \times 10^{-5}$ mol L^{-1} to 1.9×10^{-7} mol L^{-1}) at 633 nm (■) (obtained from Figure 1B) after manual fit to the line shape. (B) Magnification of plot in (A) of the relevant part of the steep slope.

results are plotted in reverse (Kc_{mon} vs Kc_T) in Figure S15 in the Supporting Information. From the obtained values α_{agg} can be calculated by using eq 10,

$$Kc_T = (1-\sigma)Kc_{mon} + \frac{\sigma Kc_{mon}}{(1-Kc_{mon})^2} \quad (9)$$

$$\alpha_{agg} = 1 - \alpha_{mon} = 1 - \frac{Kc_{mon}}{Kc_T} \quad (10)$$

and then α_{agg} values can be plotted versus the corresponding Kc_T values, which is shown in Figure 8A and in Figure S16, Supporting Information, for various σ values. The curve for $\sigma = 1$ corresponds to the isodesmic model. For $\sigma > 1$ the function describes anticooperative process of assembly (Figure S16, Supporting Information), and for $\sigma < 1$ the aggregation process is cooperative. The experimental data points for PBI **1e** are shown in Figure 8 and fitted manually for the best match. It can clearly be recognized that for small σ values (notice also the magnification in Figure 8B) the calculated curves fit very well with the experimental data, and equilibrium constants of $K_2 = 13 \pm 11$ L mol^{-1} and $K = 2.3 \pm 0.1 \times 10^6$ L mol^{-1} ($\sigma = 10^{-6} - 10^{-5}$) can be estimated within a reasonable error range. The K_2 value of the present system is in the range of equilibrium constants of dimerization by two hydrogen bonds[29] and also those of aggregating core-tetraphenoxy-substituted PBIs,[31] while the K value is significantly higher. This high K value of self-assembly of PBI **1e** can be rationalized in terms of simultaneous interaction by hydrogen bonds and $\pi-\pi$ stacking, which is only possible once the nucleus of two associated PBI dyes is formed. It cannot be evidenced yet, whether the nucleus is formed by two in-line hydrogen-bonded monomers or J-type $\pi-\pi$-stacked dimers as depicted in Figure 7B.

Circular and Linear Dichroism Studies. As shown in Figure 2, the aggregates of chiral PBI **1e** are CD active, indicating transmission of molecular side-chain chirality to the self-assembled π stack. Bisignated signals are observed in the range of S_0-S_2 transition (around 430 nm), while the signals in the S_0-S_1 transition range (660−500 nm) are monosignated. This implies that the dipole moments of the S_0-S_1 transition of the dye molecules (oriented along the long molecular axis) are parallel to each other and to the hydrogen-bonded self-assembly direction. Hence, there is no CD active coupling of these transition dipole moments, and accordingly, no bisignated signal is observable. However, the transition dipole moments of the S_0-S_2 transition, which are perpendicular to those of the S_0-S_1 transition and to the self-assembly direction, interact with each other due to a helical displacement (Figure 5G), and therefore, a bisignated signal is observed. The CD signals observed at around 300 nm are due to the twisting of the naphthalene subunits in the PBI core with one favored conformation in aggregates.[52] Upon increasing temperature the aggregates disassemble, and hence the CD signals become increasingly weaker until only monomers are present in solution at 70 °C, which is CD silent. The comparison of the CD spectrum of **1e** aggregate with that of a conformationally fixed atropisomer of alkoxy-substituted PBI reported previously[52] reveals a similar spectral shape, and $\Delta\varepsilon$ values of the strongest signal (−97 L mol^{-1} cm^{-1} at 294 nm for an atropo-enantiomeric PBI[52] and −89 L mol^{-1} cm^{-1} at 278 nm for **1e**) confirm that preferentially one-handed helical aggregates are formed in the present case.

The sign of the LD signal is indicative for whether the transition dipole moments of monomeric units within an aggregate are rather perpendicular or parallel to the orientation axis of the aggregate. Since the LD signal arises from the absorption parallel ($A_{||}$) minus the absorption perpendicular ($A_\perp$) to the orientation axis (eq 11), for parallel alignment a positive signal and for perpendicular one a negative signal is detected.

$$LD = A_{||} - A_\perp \quad (11)$$

For PBI **1a**, a positive LD signal was observed in the region of the S_0-S_1 transition which is indicative for an orientation of the monomeric dyes with an angle of less than 54.7° to the aggregate axis (Figure 3; for a quantitative analysis, it is necessary to calculate the reduced LD (LD^r); see the Supporting Information for further details). The observed negative signal in the range of the S_0-S_2 transition (which is perpendicular to the S_0-S_1 transition) corroborates this result. This again confirms our proposed model, where the monomeric PBI units are oriented with their long axis nearly parallel to the self-assembly direction.

Sergeants-and-Soldiers Studies. CD studies of mixed solutions of chiral **1e** and achiral **1d** in different ratios revealed formation of chiral heteroaggregates of these PBI dyes. It is observed that small amounts of **1e** amplify the chirality of the aggregate nonlinearly. Thus, the chiral PBI decides on the chirality sense of the whole assembly. These studies showed that already at a 30:70 ratio of chiral **1e** and achiral **1d** the CD signal is at the maximum (Figure 4B). This implies

(52) (a) Osswald, P.; Reichert, M.; Bringmann, G.; Würthner, F. *J. Org. Chem.* **2007**, *72*, 3404–3411. (b) Osswald, P.; Würthner, F. *J. Am. Chem. Soc.* **2007**, *129*, 14319–14326.
(53) De Feyter, S.; De Schryver, F. C. *Top. Curr. Chem.* **2005**, *258*, 205–255.

a dominant effect of a small fraction of chiral PBI **1e** on the chirality of heteroaggregates. Evaluation of the kinetic studies on the basis of time-dependent g values could be performed by applying an exponential relaxation function (eq 12; for derivation of this equation see the Supporting Information):

$$g(t) = g_{max} + (g_0 - g_{max}) \cdot e^{-\left(\frac{t}{\tau}\right)} \quad (12)$$

with $g(t)$, g_0 and g_{max} are the anisotropy factors at the time t, at the beginning of the measurement ($t = 0$), and at infinity, respectively, and τ is the relaxation time. The results are plotted in Figure 4C and listed in Table S1 in the Supporting Information. It is worth to point out that for mole fractions lower than 30% of **1e** the g value does not reach the maximum amplitude of -1.56×10^{-3} as values of -1.33×10^{-3} and -1.01×10^{-3} are observed for 15% and 7.5% of **1e**, respectively, at infinite time (Figure 4). This means that a certain amount of chiral component is needed to dictate the chirality for the whole supramolecular system, and this is in the present case more than 25%. In contrast, our previous studies with merocyanine dyes revealed that the calculated amplitude maxima are nearly same for 5%, 10%, and 20% of the chiral compound that were achieved after strongly varying relaxation times τ of 68.9 h, 13.9 h, and 3.1 h, respectively.[28h] For the present case, very close τ values of 4.9 h, 3.4 h, and 3.1 h were obtained for mole fractions of 7.5%, 15%, and 30%, respectively. According to our current understanding this difference between the two systems can be attributed to the different diameter of these dye assemblies. For the current PBI assemblies only two molecules constitute the nucleus (Figure 7B) which governs the chiral sense of the individual supramolecular polymer chain. In contrast, previously studied merocyanine nanorods are composed of six intertwined helically folded supramolecular chains of π-stacked dyes. It is reasonable that the tightly packed π-conjugated core of the latter is more susceptible to the chiral information imparted by the peripheral side chains but requires a longer equilibration time because the reorganization between *M*- and *P*-helicity involves more dyes.

Microscopic Studies. AFM and STM investigations revealed that dye **1a** molecules are adsorbed on HOPG substrate in long-range ordered rows within extended domains that correspond to the hexagonal symmetry of the graphite substrate (Figure 5A,B and Figure 6), which is in contrast to the fibrillar structures observed on silicon wafer substrates. HOPG is known to interact more strongly than a silicon wafer with adsorbates bearing aliphatic chains as well as aromatic π-systems,[53] and this might be the reason for the observed substrate effect on the supramolecular structures. The width of the rows on HOPG (5.7 ± 0.2 nm from AFM) corresponds well with the calculated value of the width of the monomers perpendicular to the N−N axis, which is 5.7 nm according to MM3 force field calculations. This implies a parallel orientation of the long axis of the monomers to the row direction, while the monomers are interlinked by hydrogen bonding. The fibrillar aggregates formed on silicon wafers, however, exhibit a height value of around 2 nm and a width of around 8 nm that are in reasonable agreement with the width of 5.7 and 3.0 nm for the monomers with and without alkyl chains, respectively, if one considers the tip-broadening effect.[54] This points at a helical arrangement of the monomers within the assemblies that are wrapped up by alkyl chains and adsorbed on the surface. This is assumed to cause the difficulties in determining the helical pitch and, especially, the handedness of the fibers. The values of the helical pitch are in good agreement with the calculated value of 12.0 nm obtained from molecular modeling on PBI assemblies (see Molecular Modeling section and Figure 5G).

STM measurements provided a higher resolution of the aggregates of **1a**. By considering a distance of about 0.2 nm for a hydrogen bond, our STM analysis discloses that the hydrogen-bonded chains are maintained on the HOPG surface and progress along the *b* direction of the rows (Figure 6C). The estimated distance between perylene cores (1.6 ± 0.2 nm; distance *b*) is in good agreement with the literature reported values (1.44 and 1.45 nm) obtained by STM investigations for core-disubstituted[55] and core-unsubstituted[56] perylene bisimides adsorbed on HOPG. The average length of the bright areas (1.3 ± 0.2 nm) observed in STM images of **1a** is in accord with the length of one perylene core (1.3 nm, MM3 calculation). The distance *a* between the neighboring aggregate rows (3.9 ± 0.2 nm) is expected to correlate with the molecular width, but does not agree exactly with the values calculated by MM3 method (5.7 nm) and obtained from AFM studies (5.7 ± 0.2 nm; Figure 5A,B). Presumably, the alkyl chains are partially desorbed from the HOPG surface under the influence of the solvent 1-phenyloctane.[57] In Figure 6A, the substituents can be recognized as bright horizontal lines between the rows. The angle γ in the unit cell was measured as $72 \pm 5°$ (Figure 6C). This value is pretty close to the value estimated by MM3 calculations (73°) by assuming a perpendicular orientation of the substituents referred to the N−N axis.

Conclusions

In this work, we have shown that the highly desired J-type aggregation of functional perylene bisimide chromophores can be achieved by proper design of monomeric building blocks that direct self-assembly by mutual effects of hydrogen bonding and $\pi-\pi$ interaction, and on the other hand, are prevented to assemble in columnar stacks owing to their twisted π-conjugated core. This design principle has been realized by introducing perylene bisimides **1a**−**e** that contain NH groups in the imide position to facilitate hydrogen bonding with carbonyl groups and bear bulky substituents at bay positions to disfavor H-type aggregation. The detailed studies reported here show that these appropriately designed PBI dyes self-assemble into J-aggregates with very pronounced spectral features typical for the J-type arrangement. The most outstanding functional feature of these dye assemblies is their fluorescence quantum yield of almost unity that is unprecedented among dye aggregates so far. The aggregation behavior of chiral PBI **1e** (standing exemplarily for the present PBIs) differs from that of previously reported PBIs, since the isodesmic model generally proposed for the aggregation of dyes[15a,d,23d,48] does not apply for **1e**. Rather

(54) For a discussion of the tip broadening effect on visualizing the sizes of these thin nanorods, see reference 22a.

(55) Wang, H.; Kaiser, T. E.; Uemura, S.; Würthner, F. *Chem. Commun.* **2008**, 1181–1183.
(56) (a) Ludwig, C.; Gompf, B.; Petersen, J.; Strohmaier, R.; Eisenmenger, W. *Z. Phys. B* **1994**, *93*, 365–373. (b) Cañas-Ventura, M. E.; Xiao, W.; Wasserfallen, D.; Müllen, K.; Brune, H.; Barth, J. V.; Fasel, R. *Angew. Chem., Int. Ed.* **2007**, *46*, 1814–1818.
(57) Similar observations were made for PBIs with long alkyl chains in imide positions under similar measurement conditions: Kaneda, Y.; Stawasz, M. E.; Sampson, D. L.; Parkinson, B. A. *Langmuir* **2001**, *17*, 6185–6195.

a cooperative nucleation-growth model initiated from the smallest possible nucleus of two building blocks could be confirmed for the self-assembly of PBI **1e** by concentration-dependent absorption studies. CD studies revealed that the molecular chirality of the side chains is transmitted to the self-assembled π-core and chiral heteroaggregates are formed from **1e** and achiral PBI **1d** in a dynamic aggregation process. The observed nonlinearity of chiral amplification in hetero-aggregates confirms that the sergeants-and-soldiers principle applies to these dye aggregates. The supramolecular design of formerly unprecedented arrangement of perylene bisimide dyes afforded new functional properties that are expressed in J-type excitonic coupling which holds promise for application in optoelectronic and photovoltaic devices.

Acknowledgment. We gratefully acknowledge the DFG (research training school 1221) and the Fonds der Chemischen Industrie for financial support of our work.

Supporting Information Available: General experimental information, synthetic details, and absorption and fluorescence spectra of PBIs **1a**−**e** and **2a**, temperature-dependent UV/vis spectra of PBIs **1a**−**d**, microscopic studies and ^{1}H NMR spectra of PBIs **1a**−**e**, details for data evaluation of kinetic measurements, fluorescence lifetime, calculation of the spectral shift, and plots of calculated values from LD measurement and nucleation−elongation model. This material is available free of charge via Internet at http://pubs.acs.org.

JA900684H